Mode locking in systems of globally coupled phase oscillators

Sebastian Eydam* and Matthias Wolfrum
Weierstrass Institute for Applied Analysis and Stochastic, Mohrenstrasse 39, 10117 Berlin, Germany
(Received 24 July 2017; published 7 November 2017)

We investigate the dynamics of a Kuramoto-type system of globally coupled phase oscillators with equidistant natural frequencies and a coupling strength below the synchronization threshold. It turns out that in such cases one can observe a stable regime of sharp pulses in the mean field amplitude with a pulsation frequency given by spacing of the natural frequencies. This resembles a process known as mode locking in lasers and relies on the emergence of a phase relation induced by the nonlinear coupling. We discuss the role of the first and second harmonics in the phase-interaction function for the stability of the pulsations and present various bifurcating dynamical regimes such as periodically and chaotically modulated mode locking, transitions to phase turbulence, and intermittency. Moreover, we study the role of the system size and show that in certain cases one can observe type II supertransients, where the system reaches the globally stable mode-locking solution only after an exponentially long transient of phase turbulence.

DOI: 10.1103/PhysRevE.96.052205

I. INTRODUCTION

Starting from the pioneering work of Kuramoto [1], systems of coupled phase oscillators became a fundamental paradigm for the study of the collective dynamics in coupled oscillatory systems. According to the classical theory [1,2], a large system of oscillators with heterogeneous natural frequencies under the influence of a sufficiently strong all-to-all attractive coupling undergoes a transition from a disordered state of phase turbulence to a stable regime of partial synchrony.

In this paper, we study the specific case of equidistant natural frequencies [3–5], sometimes called a *frequency comb*. It turns out that in this case already for a coupling strength below the Kuramoto threshold of transition to partial synchrony, there can appear stable states of collective order, which are characterized by sharp pulsations in the mean field amplitude occurring at a frequency close to the spacing of the natural frequencies. Due to their similarity to the regime of mode locking in lasers [6–8], we call them mode-locked solutions (MLSs), even though there can be made no direct connection between the physical mechanisms leading to mode locking in laser devices and the global mean field coupling in our Kuramoto-type model. However, the basic mechanism of establishing a phase relation between all modes without synchronizing them seems to be the same. Hence, the simple phase oscillator model can serve as a fundamental paradigm to understand in more detail the basic mechanisms of this fundamental dynamical process. Moreover, in Ref. [9] it has been pointed out how the phase dynamics of a specific optical system can be related to a—but in this case more complicated—phase-oscillator model.

The paper is organized as follows: In Sec. II the model and its mean field formulation are introduced. The notion of MLSs and the key quantities that can be used to characterize them follow in Sec. III. In Sec. IV numerical schemes are introduced. The mode-locking mechanism is discussed in detail in Sec. V. In Sec. VI the dependence of chaotic transients that precede MLSs is studied in dependence of the system size and the shape of the interaction function. In Sec. VII the parameter space is surveyed and various types of solutions are discussed. We summarize and discuss our findings in Sec. VIII.

II. THE KURAMOTO MODEL ON A FREQUENCY COMB

Our basic system consists of globally coupled phase oscillators

$$\dot{\theta}_k = \omega_k + \frac{K}{N}\sum_{j=-n}^{n}\{\gamma\sin(\theta_j-\theta_k) + (1-\gamma)\sin[2(\theta_j-\theta_k)]\}, \tag{1}$$

where $k \in \{-n,\dots,n\}$ is the oscillator index, $N = 2n+1$ is the number of oscillators, and K the coupling strength. The natural frequencies ω_k are given as a frequency comb

$$\omega_k = k\ \Delta\omega \tag{2}$$

with spacing $\Delta\omega$. In contrast to the classical Kuramoto model, we are using an attracting phase interaction function including both first and second harmonic terms [10], balanced by the additional parameter $\gamma \in [0,1]$. Normalizing the maximal natural frequency $\omega_n = 1$, such that $\omega_k \in [-1,1]$, we obtain the spacing of the natural frequencies to be $\Delta\omega = 2/(N-1)$. For convenience, we assume the number of oscillators $N = 2n+1$ to be odd and the frequency comb to be symmetric with respect to $\omega_0 = 0$.

As in Refs. [9,11], there is an equivariance of the system with respect to the transformation

$$\sigma : \theta_k \to -\theta_{-k} \quad \text{for all } k \in \{-n,\dots,n\}, \tag{3}$$

allowing for solutions with the symmetry

$$\phi_k(t) = -\phi_{-k}(t) \quad \text{for all } k \in \{1,\dots,n\}, \tag{4}$$

where $\phi_k = \theta_k - \theta_0$ is the phase difference with respect to the central mode. The distance to the symmetry-invariant subspace can be monitored by the quantity

$$\chi = \frac{1}{n}\sqrt{\sum_{k=1}^{n}(\phi_k+\phi_{-k})^2}, \tag{5}$$

*sebastian.eydam@wias-berlin.de

to detect possible symmetry breaking.

Due to our specific choice of the interaction function, one can rewrite (1) using the first and the second complex order parameter [12]

$$\eta_q(t) = R_q(t)e^{i\Psi_q(t)} = \frac{1}{N}\sum_{k=-n}^{n} e^{iq\theta_k(t)}, \quad q \in \{1,2\} \tag{6}$$

and obtain

$$\dot{\theta}_k = \omega_k - K[R_1\gamma\sin(\theta_k - \Psi_1) + R_2(1-\gamma)\sin(2\theta_k - \Psi_2)]. \tag{7}$$

The quantities R_q and Ψ_q characterize the collective behavior of the system. While $R_1(t)$ quantifies the degree of total phase synchronization, $R_2(t)$ is a measure of two cluster emergence [1,13].

III. THE NOTION OF MODE LOCKING FOR PHASE OSCILLATORS

For a given dynamical regime of the system, we can define the average effective frequencies

$$\Omega_k := \lim_{t\to\infty}\frac{1}{t}\int_0^t \dot{\theta}_k(\tau)d\tau = \lim_{t\to\infty}\frac{\theta_k(t)-\theta_k(0)}{t}, \tag{8}$$

for $k \in \{-n,\ldots,n\}$ and relative frequencies

$$\Omega_{k,j} := \Omega_k - \Omega_j \quad \text{for all } k \neq j. \tag{9}$$

For a MLS, we require that the effective frequencies form again a frequency comb,

$$\Omega_{k,k+1} = \Delta\Omega \quad \text{for all } k \in \{-n,\ldots,n-1\}. \tag{10}$$

The second property of MLSs is the formation of large pulses $R_1 \approx 1$ in the order parameter through a self-organized recurring phase relation among the oscillators. The formation of the pulse is due to the fact that after each period of $T = 2\pi/\Delta\Omega$ all oscillators meet again with nearly identical phases, while between two consecutive pulses each oscillator behaves independently, advancing its phase by exactly k clockwise round trips, where k is the oscillator index. Note that this can be achieved in a trivial way already without coupling, i.e., $K = 0$. Indeed, starting with all phases initially identical, i.e., $\theta_k(0) = 0\ \forall k$, for $K = 0$ the system will come back to this configuration after a period $T = 2\pi/\Delta\omega$. However, this trivial MLS has only neutral stability, and all other trajectories are periodic with the same period but show less pronounced or no pulsations.

The basic mechanism for mode locking is now that through the mean field coupling during the peak of $R_1(t)$ all oscillators are attracted towards the mean phase $\Psi_1(t)$, and in this way the pulsation becomes stable. Note that the coupling strength K has to remain below the synchronization threshold $K < K_C$ in order to avoid the onset of synchrony and to maintain the comb of effective frequencies.

In Fig. 1 we present numerically calculated solutions of system (1)–(2) for different parameter values and initial conditions. In Figs. 1(a) and 1(b) we show MLSs with and without the second harmonic in the interaction function. It turns out that the solution $(K,\gamma) = (1.25,0.7)$ in Fig. 1(a) is globally stable, while the solution for $(K,\gamma) = (0.91,1.0)$, shown in Fig. 1(b),

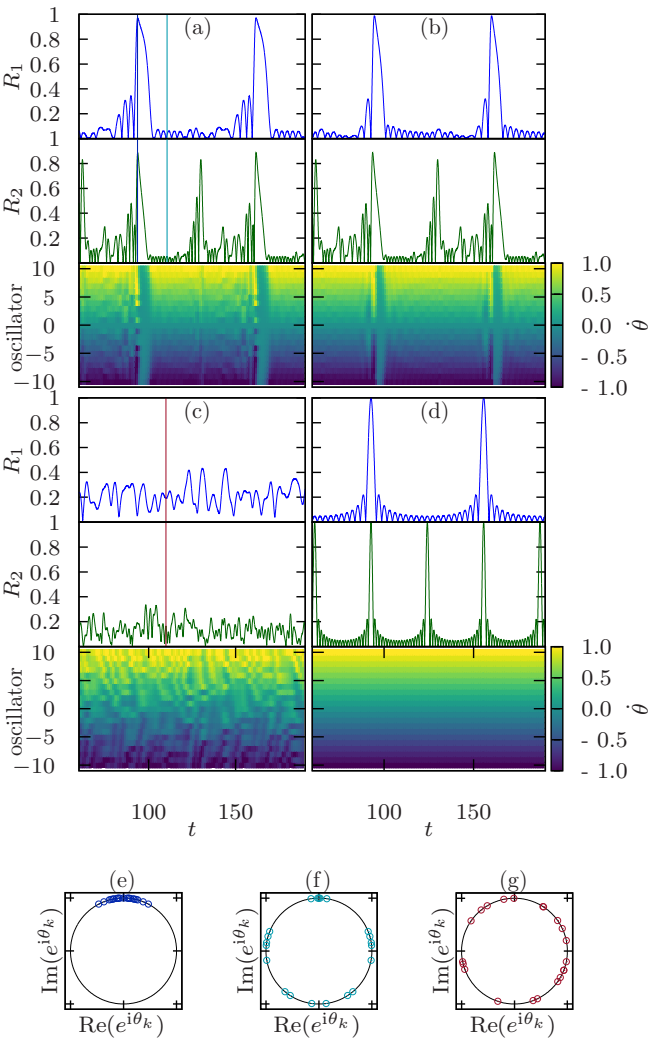

FIG. 1. Numerically calculated solutions of system (1)–(2). (a)–(d) Time evolution of mean field amplitude $R_1(t), R_2(t)$, and phase velocities $\dot{\theta}_k(t)$; (e)–(g) snapshots of the phases at the time moments indicated by vertical lines in (a) and (c). Parameter values: (a) $(K,\gamma) = (1.25,0.7)$, (b) and (c) $(K,\gamma) = (0.91,1.0)$, (d) $K = 0$. The system size is $N = 21$.

coexists with the state of phase turbulence shown in Fig. 1(c). In this case, the MLS can be found only for carefully prepared initial conditions, while the phase turbulence appears for random initial conditions. For comparison, we show the trivial MLS with $K = 0$ in Fig. 1(d), where the phase relation for the pulses is set by the initial condition rather than developed dynamically. Figures 1(e)–1(g) show time snapshots of the phases at the times indicated by colored vertical lines in Figs. 1(a) and 1(c), at the pulse, between the pulses, and in the turbulent regime, respectively. For the stable MLSs [Figs. 1(a) and 1(b)] the pulsation period is bigger than in the case of free rotation with natural frequencies [Fig. 1(d)], i.e., we find

$$\Delta\Omega < \Delta\omega.$$

The MLSs [Fig. 1(a), Figs. 1(b), and 1(d)] all carry the symmetry (4). The regime of phase turbulence for $(K,\gamma) = (0.91,1)$, shown in Fig. 1(c), has already been reported in

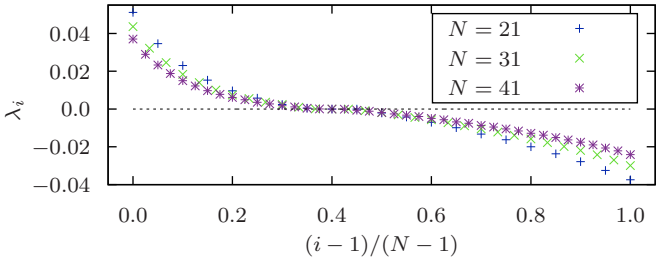

FIG. 2. Lyapunov spectra of the turbulent solutions at $(K,\gamma) = (0.91,1)$ for different system sizes $N \in \{21,31,41\}$ show extensive chaos. The time span of the computation is 2×10^5 units.

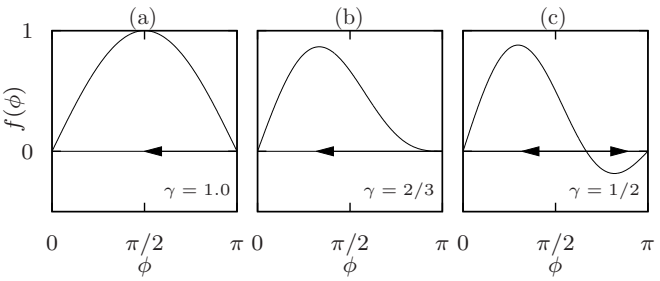

FIG. 3. Interaction between two oscillators with phase difference ϕ given by $f(\phi) = \gamma \sin(\phi) + (1-\gamma)\sin(2\phi)$ for three different values of γ. For $2/3 \leqslant \gamma \leqslant 1$ the interaction is everywhere attractive, while for $\gamma < 2/3$ it becomes repulsive for $|\phi| \approx \pi$, attracting distant oscillators to an antiphase position.

Ref. [3] where it is reported as the typical behavior of the system below synchronization, characterized by extensively chaotic Lyapunov spectra as shown in Fig. 2. Deep mathematical results on the stability of this state for random natural frequencies have been obtained only recently; see Refs. [11,14]. MLSs in the Kuramoto model right below the synchronization threshold have been reported in Ref. [15] only for very small system size $N = 5$. Note that the fluctuations between two pulses in Fig. 2(b) are considerably smaller compared to the fluctuations in the turbulent regime [Fig. 2(c)]. In Ref. [16] the mathematical framework for subharmonic locking of several oscillators in a more general setting has been elaborated.

IV. NUMERICAL METHODS

For all simulations we use a fourth order Runge-Kutta method with a step size of $h = 0.01$. Since simulations of a flow on $\mathbb{T}^N$ are usually performed on the universal cover $\mathbb{R}^N$ one has to regularly project back to the unit circle interval in order to avoid digit cancellation in long simulations. To investigate MLSs we use Poincaré events given by the condition

$$\theta_k - \theta_{k+1} = 0 \tag{11}$$

for some $k \in \{-n, \ldots, n-1\}$ and record the return times T_ν between successive Poincaré events. The Poincaré condition is typically met once per pulse for a MLS, however, not necessarily close to the pulse itself. In parameter scans, where system parameters are changed adiabatically, we take care of possible numerical trapping in invariant subspaces induced by symmetry by adding small perturbations to the initial state after each adaption of the parameters. Lyapunov exponents are computed via a continuous Gram-Schmidt orthonormalization procedure as has been described in Ref. [17].

V. THE ROLE OF FIRST AND SECOND HARMONICS IN THE INTERACTION FUNCTION

As mentioned before, there is a fundamental difference between the case $\gamma = 1$ of only the first harmonic in the interaction function and the case of a second harmonic added to the interaction function. For $\gamma = 1$, almost all initial conditions lead to the turbulent state and only specifically chosen initial conditions lead to a MLS; cf. Fig. 1. The presented solution has been obtained by choosing a fully synchronized solution found for $K > K_C$ as initial condition. Moreover, for $\gamma = 1$ the MLS is extremely fragile and sensitive to perturbations.

In contrast to that for suitably chosen γ the MLS solution is globally stable. In Sec. VI we present numerical results showing that for values of γ in a range around 0.7 MLSs appear starting from any random initial condition. It turns out that the mode-locking mechanism is most efficient for $\gamma \approx 2/3$, where the interaction of oscillators with a phase difference $|\theta_j - \theta_k|\pi$ is particularly weak; cf. Fig. 3. Note that for $\gamma < 2/3$ there appears already a repulsive interaction of distant oscillators, forcing them towards an antiphase position and in this way inhibiting the mode-locking mechanism.

Another feature of the MLSs is the appearance of pulses in the second order parameter $R_2(t)$. They appear at the position of the pulse in the mean field $R_1(t)$ and additionally in the middle between two such pulses. Note that for the trivial case of $K = 0$ and $\theta_k(0)$ for all k [see Fig. 1(d)] we get $R_2(T/2) = 1$. During such intermediate pulses in $R_2(t)$ the second harmonic term in (7) dominates, and the oscillators are attracted to the two antiphase positions $\Psi_2(t)$ and $\Psi_2(t) + \pi$. It turns out that this process has a substantial impact on the stability of the MLS.

In order to understand the impact of the pulses in the mean fields $R_1(t)$ and $R_2(t)$ for the stability of the MLS, we present now a time-resolved computation of the attraction along the mode-locked periodic orbit. For stable periodic orbits both the leading Floquet exponent, giving the averaged rate of attraction (repulsion) of nearby trajectories, and the averaged rate of expansion (contraction) of phase space volume are negative. In the case of stable MLS the time-resolved quantities show most of the time a slight repulsion and of nearby trajectories and an expansion of phase space volume that, however, overall is compensated by strong attraction an contraction of phase space volume during the short pulses in the mean fields. In Fig. 4 we compare the instantaneous stability along the MLS both for the case $(K,\gamma) = (0.91,1.0)$, where the MLS coexists with phase turbulence, and for the globally stable case at $(K,\gamma) = (1.25,0.7)$. Together with the time traces of the order parameters we show the instantaneous expansion rate of the phase space volume

$$\Lambda(t) = \sum_{i=1}^{N} \lambda_i(t) \tag{12}$$

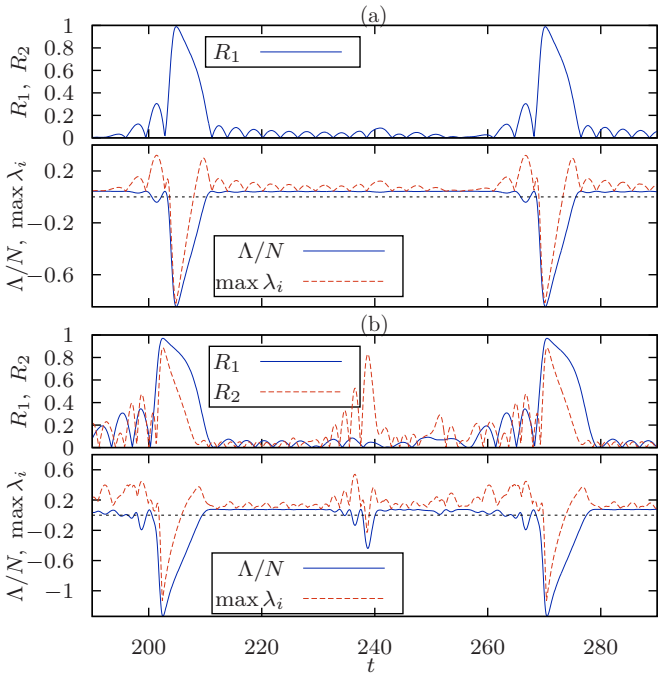

FIG. 4. Time traces of order parameters $R_{1,2}$ (upper rows) together with normalized expansion rate of phase space volume $\Lambda(t)/N$ and maximal instantaneous eigenvalue $\max\lambda_i(t)$. (a) MLS with first harmonic interaction $(K,\gamma) = (0.91,1.0)$ [here only $R_1(t)$ is relevant]; (b) MLS with second harmonic interaction $(K,\gamma) = (1.25,0.7)$.

given for each time t as the sum of the eigenvalues $\lambda_i(t)$ of the Jacobian along the MLS and the maximal instantaneous eigenvalue $\max\lambda_i(t)$. One can see in panel (a) that for $\gamma = 1$ there is a uniform level of volume expansion between the pulses and only at the mode-locked pulse the expansion rate and eventually all instantaneous eigenvalues become negative. This is different for the case with second harmonic interaction, shown in panel (b). While in the first part of the interpulse interval the stability properties are similar to the case of $\gamma = 1$, there appears another episode of volume contraction and instantaneous stability at the pulse in $R_2(t)$, and after this event the uniform level of volume expansion starts to disappear. In both cases, the stability of the MLS originates from a strong contraction during the pulse events, while over a large part of the period there is a volume expansion, inducing locally a growth of generic perturbations from the MLS. In the case with second harmonic interaction the contraction acts also during the pulse in $R_2(t)$ and in this way enhances substantially the stability and of the whole periodic orbit. In a similar way, additional higher harmonics could possibly have a further positive impact on the stability.

VI. CHAOTIC SUPERTRANSIENTS

Also for values of γ where the MLS are globally stable, they can be difficult to find in numerical simulations, because using random initial conditions the average transient time before the system reaches a MLS increases drastically with the system size. Figure 5 shows in a logarithmic plot the average transient

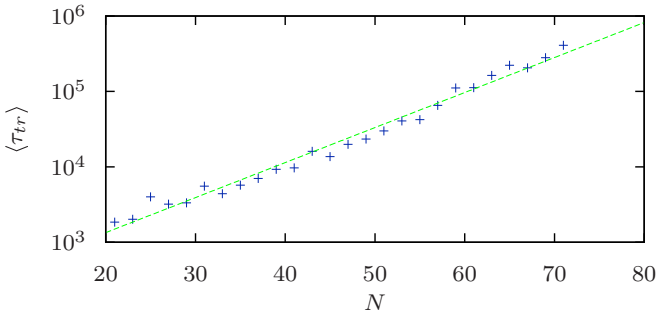

FIG. 5. Logarithmic plot of the average transient time from random initial conditions to the stable MLS, varying the system size N. Averages are taken for $N \leqslant 53$ over 300 realizations of initial conditions. For larger N, their number had to be restricted to 50. Parameters: $(K,\gamma) = (1.2, 0.7)$.

time $\langle\tau_{\rm tr}\rangle$ from random initial conditions to the stable MLS varying the system size N. At the chosen parameters $(K,\gamma) = (1.2,0.7)$ all random initial data were found to converge to the MLS. Remarkably, we find that the average time spent on a chaotic transient, similar to the regime of phase turbulence observed for $\gamma = 1$, scales exponentially with the system size

$$\langle\tau_{\rm tr}\rangle \propto e^{\kappa N}, \tag{13}$$

with the coefficient $\kappa \approx 0.11$. The transients can be classified as type II chaotic supertransients [18,19], i.e., the transition from incoherence to the MLS is abrupt rather than gradual. Qualitatively, this scaling behavior can be explained by interpreting the nonlinear regime of phase turbulence as a random process, taking the phase configurations eventually into a certain small neighborhood of a MLS, where the linear stability dominates the nonlinear processes. The exponential scaling is then given by the average time that a random trajectory needs to reach a specific volume in $\mathbb{T}^N$, growing exponentially with N as well. The parameter γ in the interaction function has a substantial influence on the transient times. In Fig. 6 the average transient time in dependence of γ is shown for different system sizes N and coupling strengths K. Each point represents the average over 200 different initial conditions. The computations were stopped in the case of large periods as in modulated solutions and also when a transient exceeded 10^6 time units. Results are shown only for parameters where

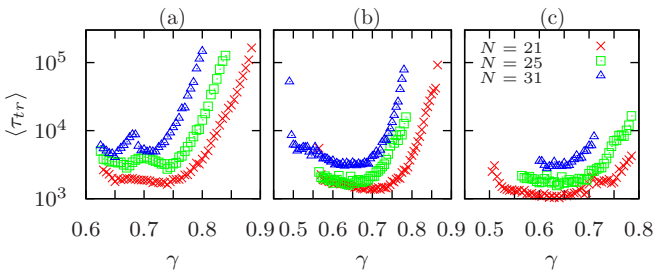

FIG. 6. Average transient times in logarithmic plot for varying γ. Coupling strength $K = 1.2, 1.25, 1.3$, panels (a), (b), (c), respectively. Symbols and colors indicate different system sizes $N \in \{21,25,31\}$. Each point represents an average over 200 random initial condition.

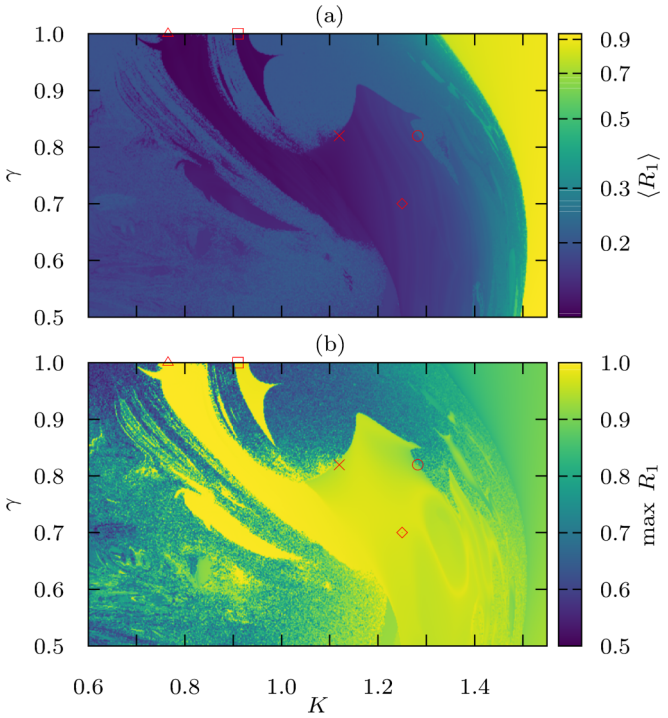

FIG. 7. For a system of $N = 21$ the average and maximal order parameter are shown in (a) and (b), respectively. As initial conditions we used synchronous solutions obtained for $K > K_C$. Marked points correspond to parameter values of examples shown in other figures: ◇ = globally stable MLS, see Fig. 4 (b); □ = stable MLS coexisting with turbulence, see Fig. 4 (a); △ = modulated MLS (comb splitting), see Fig. 9; ○ = torus breakup, see Fig. 10; × = intermittent solution, see Fig. 11.

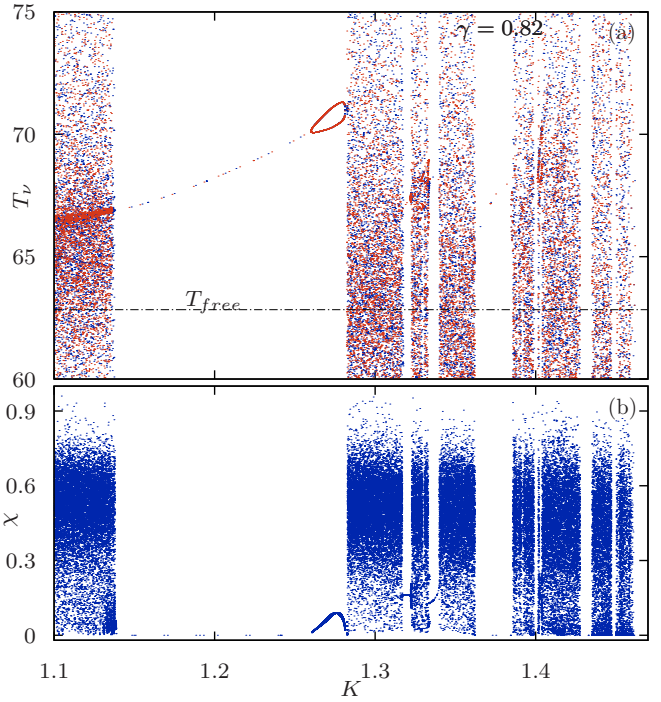

FIG. 8. (a) Sampled return times T_ν for varying parameter K,$\gamma = 0.82$. Different colors correspond to increasing (blue) and decreasing (orange) coupling strength. Narrow periodic windows occur between regions of phase chaos. (b) Sampled distances χ from the symmetry-invariant subspace with respect to the symmetry action σ at the crossings of the section.

a stable MLS was reached for all initial conditions within 10^6 time units. As we will see below, there are parameter values where more complicated types of periodic solutions and multistability between them may exist. As γ increases, i.e., for the first harmonic dominating, the transient times show an exponential growth before the MLS loses its stability.

VII. INSTABILITIES AND BIFURCATIONS

Varying parameters K and γ, we observe an extremely complicated scenario of coexistence and transitions between different dynamical regimes, containing not only stable MLSs and phase turbulence but also a variety of more complicated solutions emerging from the fundamental MLS. In Fig. 7 a survey for different parameter values K,γ is presented, using coherent initial conditions from the synchronous state, which appears for coupling strength $K > K_C$ above the Kuramoto threshold. The different levels of the average order parameter, given in Fig. 7(a), allows us to distinguish between synchrony (values close to one), phase chaos (intermediate values), and mode locking (smallest values). The maximal values of the order parameter, given in Fig. 7(b), indicate high coherence at the mode-locking peaks and allow us to identify also those regions where such peaks appear erratically.

The parameter scan in Fig. 8 for $\gamma = 0.82$ shows that various symmetric and asymmetric MLSs as well as chaotic regions appear for varying coupling strength K. In the following subsections we discuss some of the more complicated types of solutions and some of the transition scenarios in more detail. A comprehensive bifurcation analysis in the two parameters K and γ would be desirable but seems to be beyond the scope of the present paper.

A. Modulated mode-locked solutions

In the regime of fundamental mode locking reappearing pulses are identical, and the period is the time between two pulses. In addition, we observe solutions where the effective frequencies Ω_k are still equidistant, but the pulse heights and interpulse intervals are modulated. This modulation can be periodic, quasiperiodic, or chaotic. The transitions are mediated by period doubling or torus bifurcation resulting in periodic or quasiperiodic modulation, respectively. Subsequently chaotically modulated MLSs can arise via torus breakup or period doubling cascades.

B. Comb splitting

It turns out that in our setting of equidistant natural frequencies there can appear more complicated configurations of the effective frequencies Ω_k. In particular, we observe a specific type of solution where two different spacings $\Omega_{k,k+1} \in \{\Delta\Omega_1, \Delta\Omega_2\}$ between the effective frequencies appear as a result of dynamical self-organization. If the spacings show a rational relation $p\Delta\Omega_1 = q\Delta\Omega_2$ with $p,q \in \mathbb{N}$, the solution

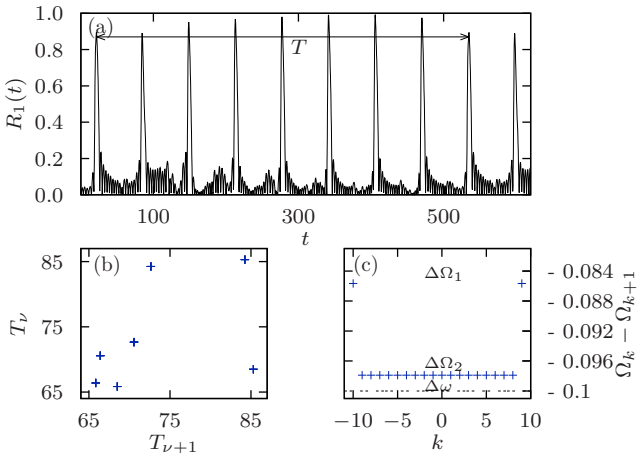

FIG. 9. Comb splitting MLS for $(K,\gamma) = (0.765, 1.0)$ and $N = 21$. (a) Time trace of the order parameter $R_1(t)$; (b) orbit of period 7 in a two-dimensional Poincaré section with return times T_ν of consecutive section crossings plotted against each other; (c) spacings $\Delta\Omega$ of effective frequencies.

is periodic with period

$$T = 2\pi p/\Delta\Omega_1 = 2\pi q/\Delta\Omega_2.$$

An example for first harmonic coupling $\gamma = 1$ with a rational relation of the two spacings is shown in Fig. 9. From the evolution of $R_1(t)$, shown in Fig. 9(a), one can clearly see a modulation of the pulses. Consecutive interpulse intervals obtained from the return times between crossings of the Poincaré section are plotted in Fig. 9(b). Note that the number of section crossings during a period with a split frequency comb depends on the frequency spacing between the two oscillators that are used for the section. In Fig. 9(c) we show the effective frequency spacings that are related here by the ratio 7/8. When the ratio between the two spacings is irrational the solution has a quasiperiodic modulation. In that case one finds a closed curve in the two-dimensional Poincaré section instead of multiple points.

C. Torus breakup chaotically modulated MLS, symmetry breaking, and multistability

A scenario leading from a fundamental MLS towards more complicated solutions is shown in Fig. 10. A harmonic MLS undergoes a torus bifurcation with a subsequent breakup of the invariant torus and emergence of chaos. In Fig. 10(a) we have sampled the Poincaré return times for varying coupling strength K, where the two different colors blue and orange correspond to sweeping in positive and negative directions, respectively. In a two-dimensional Poincaré section, shown in Fig. 10(b), we observe the emergence of a closed curve. For further increasing K, this curve folds over, and after the breakup of the corresponding invariant torus, a chaotic attractor appears; see Fig. 10(c). This chaotic attractor collapses via cascade of period doublings to a period 5 solution at slightly higher values of K; see Fig. 10(a). Here two stable periodic solutions with five pulses per period coexist. These solutions do not have the symmetry (4) anymore. Instead they show up

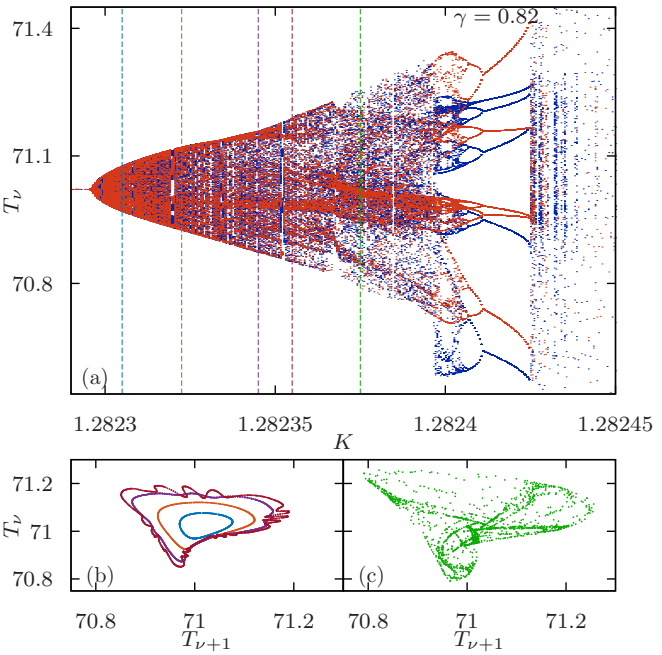

FIG. 10. (a) Sampled return times T_ν between crossings of the Poincaré section (11) for $\gamma = 0.82$ and varying K; blue and orange correspond to sweeping K in the increasing and decreasing directions. (b) and (c) Two-dimensional representation of return times T_ν for selected values of K given by dashed lines in panel (a). Closed curves in (b) represent invariant tori. Low-dimensional chaos in (c).

as a symmetry-related pair $\phi(t)$ and $\tilde{\phi}(t)$, satisfying

$$\phi_k(t) = -\tilde{\phi}_{-k}(t). \tag{14}$$

Since our Poincaré condition (11) is not invariant under the symmetry action (3), we get different return times for $\phi(t)$ and $\tilde{\phi}(t)$, which can be distinguished by the two different colors in the period 5 window in panel (a). For further increasing K the period 5 orbit disappears in an intermittency transition as discussed in more detail in the next section.

D. Intermittency between phase turbulence and MLS

In addition to the transition from MLSs to low-dimensional chaos as discussed above, we can also observe direct transitions to extensive chaos. This happens when a MLS or modulated MLS loses its stability and an intermittent behavior [20,21] appears, alternating between phase chaos and episodes

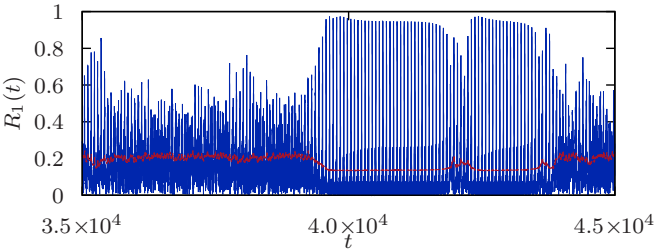

FIG. 11. Time trace of $R_1(t)$ at $(K,\gamma) = (1.12, 0.82)$, showing intermittency between phase chaos and a MLS. The rolling average (15) can be used to distinguish between the two regimes (red line).

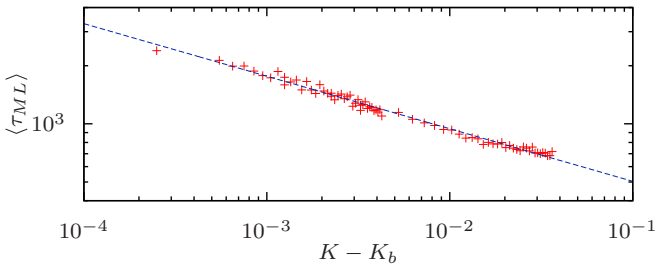

FIG. 12. Distance from the critical parameter K_b and average fraction of mode locking $\langle \tau_{\mathrm{ML}} \rangle$ in a double logarithmic plot.

close to the weakly unstable MLS. As an example, we analyze the intermittent behavior in the parameter window below $K = 1.137$ for $\gamma = 0.82$. A time trace of $R_1(t)$ in this intermittent regime is shown in Fig. 11. It turns out that the two alternating regimes can be characterized by the rolling average of R_1 for a time window of length T close to the approximate interpulse interval of the underlying MLS:

$$\langle R_1(t) \rangle_T = \frac{1}{T} \int_{t-T}^{t} R_1(\tau)\, d\tau. \tag{15}$$

This quantity, shown by the red line in Fig. 11, is almost constant when the system is close to the MLS and is fluctuating around a significantly higher value in the regime of phase chaos. In this way, we can extract from our numerical solutions the average fraction of mode locking $\langle \tau_{\mathrm{ML}} \rangle$ in the intermittent trajectories. Varying the coupling parameter close to its critical value $K_b \approx 1.137$ we obtain a power law

$$\langle \tau_{\mathrm{ML}} \rangle \propto |K - K_b|^{-\alpha}, \tag{16}$$

shown in Fig. 12, which is typical for intermittency transitions. From this we can extract the critical exponent $\alpha \approx 0.27$, which can be related to properties of the unstable peroidic orbit; see Ref. [22].

VIII. CONCLUSION

We have introduced the notion of mode locking for coupled phase oscillators and demonstrated this phenomenon in globally coupled systems of Kuramoto-Daido type with equidistant natural frequencies. Already below the Kuramoto threshold this leads to a stable collective dynamical regime, characterized by sharp periodic pulses in the global mean field. Their stability can be substantially enhanced by introducing a second harmonic in the coupling function. In this case, for suitably chosen parameters the MLS is globally stable. For classical Kuramoto oscillators, i.e., with only the first harmonic in the coupling function, they are difficult to find, since they can be found only in coexistence with stable phase chaos. Also in the cases where the MLS is globally stable, the transient times from random initial conditions to the MLS grow exponentially with the number of oscillators, while before this transition type II supertransients of phase chaos are observed. In addition to the fundamental MLS, we demonstrate also the existence of various types of modulated MLSs and study the transitions between them. In particular, we observe an intermittent behavior between the extensive chaos of phase turbulence and the periodic regime of mode locking.

We believe that the concept of mode locking represents another fundamental mechanism for the emergence of self-organized collective dynamics in systems of coupled oscillators. A study of this phenomenon in systems of simple phase oscillators of Kuramoto type can give insight into the relevant mechanisms of the phase dynamics, which we have shown to be characterized by complex and high-dimensional dynamical phenomena.

To which extent these insights can be used for a better understanding of the already extensively studied process of mode locking in laser systems remains an open question for future studies. Major differences to dynamical models for mode locking in laser devices [7,8] is that there the coupling of the modes is not given directly by a mean field of the oscillators, but is mediated by additional dynamical quantities such as gain and absorption. Moreover, the dynamics of the mode amplitudes, which are fixed to be constants in our phase oscillator model, are considered to play an important role there.

ACKNOWLEDGMENT

The authors acknowledge the support by Deutsche Forschungsgemeinschaft in the framework of Collaborative Research Center SFB 910.

[1] Y. Kuramoto, *Chemical Oscillations, Waves, and Turbulence*, Springer Series in Synergetics (Springer, New York, 1984).
[2] A. Pikovsky, M. Rosenblum, and J. Kurths, *Synchronization: A Universal Concept in Nonlinear Sciences*, Cambridge Nonlinear Science Series, Vol. 12 (Cambridge University Press, Cambridge, 2003).
[3] O. V. Popovych, Y. L. Maistrenko, and P. A. Tass, Phys. Rev. E **71**, 065201(R) (2005).
[4] D. Pazó, Phys. Rev. E **72**, 046211 (2005).
[5] B. Ottino-Löffler and S. H. Strogatz, Phys. Rev. E **93**, 062220 (2016).
[6] H. A. Haus, J. Appl. Phys. **46**, 3049 (1975).
[7] A. G. Vladimirov and D. Turaev, Phys. Rev. A **72**, 033808 (2005).
[8] E. A. Avrutin, J. M. Arnold, and J. H. Marsh, IEEE J. Sel. Top. Quantum Electron. **9**, 844 (2003).
[9] Y. H. Wen, M. R. E. Lamont, S. H. Strogatz, and A. L. Gaeta, Phys. Rev. A **94**, 063843 (2016).
[10] D. Hansel, G. Mato, and C. Meunier, Europhys. Lett. (EPL) **23**, 367 (1993).
[11] H. Chiba and D. Pazó, Physica D **238**, 1068 (2009).
[12] H. Daido, Physica D **91**, 24 (1996).
[13] M. Komarov and A. Pikovsky, Phys. Rev. Lett. **111**, 204101 (2013).
[14] H. Dietert, J. Math. Pures Appl. **105**, 451 (2016).
[15] Y. L. Maistrenko, O. V. Popovych, O. Burylko, and P. A. Tass, Phys. Rev. Lett. **93**, 084102 (2004).

[16] C. Baesens, J. Guckenheimer, S. Kim, and R. Mackay, Physica D **49**, 387 (1991).
[17] F. Christiansen and H. H. Rugh, Nonlinearity **10.5**, 1063 (1997).
[18] C. Grebogi, E. Ott, and J. A. Yorke, Ergodic Theory Dyn. Syst. **5**, 341 (1985).
[19] T. Tél and Y.-C. Lai, Phys. Rep. **460**, 245 (2008).
[20] J.-P. Eckmann, Rev. Mod. Phys. **53**, 643 (1981).
[21] Y. Pomeau and P. Manneville, Comm. Math. Phys. **74**, 189 (1980).
[22] E. Ott, *Chaos in Dynamical Systems*, 2nd ed. (Cambridge University Press, Cambridge, 2002).